ELSEVIER

Remote Sensing of Environment 79 (2002) 279–287

Remote Sensing of Environment

www.elsevier.com/locate/rse

Radiometric slope correction for forest biomass estimation from SAR data in the Western Sayani Mountains, Siberia

G. Sun[a,*], K.J. Ranson[b], V.I. Kharuk[c]

[a]*Department of Geography, University of Maryland, College Park, MD 20742, USA*
[b]*NASA's Goddard Space Flight Center, Code 923, Greenbelt, MD 20771, USA*
[c]*Sukachev Institute of Forest, Krasnoyarsk, Russia*

Received 18 April 2000; received in revised form 15 December 2000; accepted 28 February 2001

Abstract

We investigated the possibility of using multiple polarization (SIR-C) L-band data to map forest biomass in a mountainous area in Siberia. The use of a digital elevation model (DEM) and a model-based method for reducing terrain effects was evaluated. We found that the available DEM data were not suitable to correct the topographic effects on the SIR-C radar images. A model-based slope correction was applied to an L-band cross-polarized (hv) backscattering image and found to reduce the topographic effect. A map of aboveground biomass was produced from the corrected image. The results indicated that multipolarization L-band synthetic aperture radar (SAR) data can be useful for estimation of total aboveground biomass of forest stands in mountainous areas.

Keywords: Forest biomass; Terrain effect; SAR; Backscatter model

1. Introduction

Several authors have developed methods and algorithms for mapping aboveground biomass in the boreal forest (Beaudoin, et al., 1994; Bergen, Dobson, Pierce, & Ulaby, 1998; Dobson et al., 1992, 1995; Kurvonen, Pulliainen, & Hallikainen, 1999; Le Toan, Beaudoin, Riom, & Guyon, 1992; Paloscia, Macelloni, Pampaloni, & Sigismondi, 1999; Ranson, Saatchi, & Sun, 1995; Ranson & Sun, 1997a; Rignot, Way, Williams, & Viereck, 1994; Saatchi & Moghaddam, 2001; Saatchi, van Zyl, & Assar, 1995). These studies concentrated on relatively flat areas, where terrain effects were not significant. Estimation of forest biomass using synthetic aperture radar (SAR) data can be complicated by topography that influences radar backscatter (Bayer, Winter, & Schreier, 1991; Luckmanm, 1998; Rauste, 1990; van Zyl, 1993), particularly through local incidence angle, shadowing, and effects on radar backscattering can be complex. Changes in radar incidence angle caused by terrain slope can have several effects on radar image data. For example, radar backscattering varies with incidence angle, which varies with terrain slope and aspect. Foreshortening is also a terrain-induced effect where a smaller incidence angle results in more ground surface area being illuminated. If the terrain slope is larger than the radar incidence angle, layover occurs and the backscattering from the slope will mix with the signature from other targets. When a slope faces away from the radar and the slope is steeper than the incidence angle, shadowing occurs. There is no way to recover the signatures lost due to layover and shadowing. Another effect of terrain on the backscatter is the apparent change of the forest spatial structure in the radar field of view. For example, when trees of a relatively uniform stand grow on a slope, a portion of the sides of these trees will be directly exposed to the radar beam.

Terrain correction techniques are designed to reduce effects of incidence angle and illuminated target area. For correction of the illuminated pixel area, simple algorithms can be used if a suitable digital elevation model (DEM) exists (Kellndorfer, Pierce, Dobson, & Ulaby, 1998; Shi & Dozier, 1997). Correction of the backscattering dependence on incidence angle requires knowledge of the land cover

* Corresponding author. Tel.: +1-301-614-6655; fax: +1-301-614-6695.
E-mail address: guoqing@aspen.gsfc.nasa.gov (G. Sun).

0034-4257/01/$ – see front matter
PII: S0034-4257(01)00279-6

type within a pixel. A few attempts have been made to correct terrain effects by using simple radar backscattering models and a DEM. For example, Goering, Chen, Hinzman, and Kane (1995) used a DEM and empirical radar backscatter models to reduce terrain effects from ERS-1 SAR images. However, Goyal, Seyfried, and O'Neill (1998) found that the small-scale topographic features resolved by SAR could not be resolved by a DEM in rugged terrain. Periodic artifacts due to the terrain model generation methodology were observed in the derived variables (e.g., slopes). Other methods, such as image ratios, were used to reduce the effects of radar incidence angle caused by topography (Ranson, Saatchi, & Sun, 1995; Ranson, Sun, Kharuk, & Kovacs, 2001; Shi & Dozier, 1997; Wever & Bodechtel, 1998). Wever and Bodechtel (1998) proposed the use of L-band hv (Lhv) and X-band VV (Xvv) ratio or difference images for radiometric rectification. Ulander (1996) described a new equation for radiometric slope correction using the slope information derived from the SAR interferograms.

In the work reported herein, we discuss the correction for the dependence of illuminated pixel area on incidence angle using a DEM. We then present a method to correct for the backscatter dependence on terrain using a model to simulate radar backscattering of a forest stand on various slopes. The derived dependence of the Lhh and Lhv backscattering on radar local incidence angle was used to remove the terrain effect from the Lhv data. Finally, a biomass map was produced from the corrected Lhv data.

2. Study area

This work utilized ground measurements and SAR data from a mountainous area in central Siberia, Russia. The test area, in the Western Sayani Mountains covers a 50×25 km area with center coordinates of 53°4.2′N latitude and 93°14.3′E longitude. The area is part of the dark-coniferous taiga forests that grow in mountainous regions (300–1400 m above mean sea level). The forests of this area include Siberian cedar (*Pinus siberica*) and fir (*Abies sibirica*), with few stands of aspen (*Populus tremula*) and birch (*Betula verrocosa*). The climate is continental with wet summers and cold dry winters. Temperature and precipitation patterns are strongly influenced by elevation. Annual precipitation varies from 560 mm in the lower regions to 1300 mm at higher elevations. Tree line occurs at about 1400 m elevation. The area is the site of the Ermakovsky Permanent Study Area established in 1959 and used for research by the Sukachev Institute of the Siberian Branch of the Russian Academy of Sciences.

A Russian forest inventory map (1:50,000) compiled from aerial photographs and site visits between 1993 and 1995 was used as ground truth information. The map is typical of forest inventory maps with forest units related to economic value of the stands. Table 1 lists the biomass data for sites used in this study.

Table 1
Field biomass (kg/m^2) of the forest stands used in this study

Model		Testing	
Plot	Biomass	Plot	Biomass
2	1.16	1	1.16
4	2.00	3	1.16
6	3.66	5	2.70
8	3.66	7	3.66
10	3.66	9	3.66
12	3.66	11	3.66
14	3.85	13	3.85
16	4.24	15	3.85
18	4.92	17	4.92
20	5.61	19	5.07
22	5.61	21	5.61
24	6.75	23	5.67
26	7.56	25	7.35
28	8.04	27	8.04
30	10.00	29	8.30
32	11.23	31	11.02
34	14.60	33	13.34
36	17.50	35	17.50
38	18.80	37	17.52
40	18.80	39	18.80
42	18.80	41	18.80
44	19.40	43	19.40
46	19.40	45	19.40
48	19.40	47	19.40
50	19.40	49	19.40
52	19.40	51	19.40
54	22.20	53	20.00
56	24.00	55	22.20

Even number stands were used to develop a regression model, and odd numbered stands were used for testing.

3. SIR-C/XSAR data

Shuttle Imaging Radar/ X-band SAR (SIR-C/XSAR) data were used in this study. The SIR-C/X-SAR missions were flown during April 9–19, 1994 and September 30–October 10, 1994 (Stofan et al., 1995). The instrument had quad-polarized (hh, hv, vv, vh) L-band (wavelength = 23 cm) and C-band (5.6 cm) radar and vv polarized X-band (3 cm) radar channels. The mission was a cooperative experiment between NASA's Jet Propulsion Laboratory (JPL), the German Space Agency, and the Italian Space Agency. The SIR-C image data used in this study were acquired on April 16, 1994 with an image center incidence angle of 46.4°. The original image is single look complex data with line spacing (azimuth) of 5.8 m and pixel spacing (slant range) of 13.3 m. The images were processed with six looks in azimuth and two looks in range direction resulting in images with a pixel size of $\sim$35 m.

Since previous work (Dobson et al., 1995; Ranson et al., 1995; Ranson & Sun, 1997b) had shown that Lhv data is

Fig. 1. Original SIR-C Lhv image of the study area in Western Sayani Mountains, Siberia.

especially sensitive to forest aboveground biomass, only L-band data were used in this study. Fig. 1 is the Lhv image of the study area. In the image, the Sayani Mountains can be seen on the left side of the image. Forested mountains appear bright or dark depending on the slope and aspect with respect to the radar illuminating direction (from right of this image). Some deforested areas are evident in the center of the image. A broad level plain to the right has large wetland areas such as the dark object in the lower right corner and bare agricultural fields. The village of Ermakovsky and the Sukachev Institute of Forest field camp are located at the upper right on this image.

4. Methods

4.1. Terrain effects correction using a DEM

The DEM available for use was Digital Terrain Elevation Data (DTED) Level 1 (three arc second pixel spacing) from the U.S. Department of Defense. The DEM offers a pixel spacing of roughly 100×60 m at the study area and a nominal accuracy of ± 30 m. Because the pixel size of the SAR image is about 35 m, the DEM was interpolated and used to simulate a SIR-C SAR image using the platform and image parameters provided by JPL. The SIR-C images were then registered to this simulated image and the elevation was obtained for each SIR-C image pixel. Slope and aspect were then generated from these elevations and used to calculate the local incidence angle for every pixel of the image as Eq. (1):

$$\cos(\theta) = \sin(\alpha_s)\sin(\alpha)\cos(\beta - \beta_s) + \cos(\alpha_s)\cos(\alpha) \quad (1)$$

where θ = local incidence angle, α_s = local slope angle, α = zenith angle of the SAR platform, β_s = aspect of slope, and β = azimuth angle of the SAR platform.

Radiometric distortion due to the illumination areas was corrected using the local incidence angle with an equation (Eq. (2)) of the form used by Kellndorfer et al. (1998).

$$\sigma^\circ_{\text{corr}} = \sigma^\circ \sin(\theta)/\sin(I_{\text{ref}}) \quad (2)$$

where: $\sigma^\circ_{\text{corr}}$ = radar backscatter coefficient corrected for local incidence angle, σ° = original backscatter coefficient; θ = local incidence angle at each pixel, and I_{ref} = the radar incidence angle at the center of the image.

Kellndorfer et al. (1998) found that this correction was adequate for land cover classification purpose. The radar backscattering is a function of incidence angle, and different types of terrain have different dependence on the radar incidence angle. Different backscattering models are required to make this correction. It might be possible to model the dependence of backscattering on local radar incidence angle if the detailed knowledge of the forest types and their structure information are known. This was not feasible in this study since data for several of the local species in the area were not available. Rather, the radar model was parameterized with general forest structure information and then used to correct terrain effects as discussed below.

4.2. Modeling radar backscatter of forest stands on slopes

The 3-D radar backscatter model (Sun & Ranson, 1995) was modified for this study to include the effect of slopes on backscatter. The modified model accepts a stem map (with location, diameter breast height (dbh), height, species, and crown shape for each tree), an elevation map (height for each surface pixel), and a soil surface roughness and dielectric constant map as inputs to simulate high-resolution polarimetric radar images of the forest stand. The scattering components are also available from the modeling outputs. Detailed measurements of the forest structure were not available for the Western Sayani Mountain study area. We used measurements acquired for a boreal conifer stand in Canada to parameterize the 3-D model to simulate radar backscattering for trees growing on various slopes. A 100×100 m stem map within a mature jack pine (*Pinus*

banksiana) stand was made during the Boreal Ecosystem–Atmosphere (BOREAS) Study (Sellers et al., 1998) in 1994. The measurements included the stem locations, dbh, species, and relative canopy positions (e.g., dominant, codominant, intermediate, suppressed) for 1900 trees in the stand. This stand is a typical boreal conifer forest with aboveground dry biomass of about 10 kg/m^2. In addition to the stem map, total height, crown length, and crown width were measured for many jack pine trees as part of other BOREAS field activities. The relationships between these parameters and dbh were developed from the field measurements. These relationships were then used with the stem map dbh data to infer tree crown characteristics for each tree. When a slope was introduced, the horizontal position of a tree was not changed, but the tree was vertically moved depending on its position within the stand. Tree crowns were modeled as cones. The backscattering from the ground surface was calculated using the integral equation model (Fung, 1994). The parameters for the simulation are listed in Table 2.

Since Lhh backscatter is more sensitive to slope (i.e., has greater canopy penetration and so sees more ground), it was used to estimate the local incidence angle (θ). Then $\cos\theta$ was used to correct the Lhv image. To do so, a simple analytical relationship between backscattering coefficients and incidence angle needed to be established for both hh and hv polarizations.

The simple backscattering models for vegetation-like media take the form of:

$$\sigma^\circ(\theta) = \sigma^\circ \cos^p \theta.$$

where θ is the local incidence angle (Ulaby, Moore, & Fung, 1982). Both σ° and p are polarization dependent. When $p=1$, the model means that the scattering coefficient (scattering per unit surface area) is dependent on $\cos\theta$, which is the ratio of projected area (normal to the incoming rays) to the surface area. When $p=2$, the model is based on Lambert's law for optics. Ulaby et al. (1982) pointed out that although either $p=1$ or 2 seldom closely approximate the real scattering, sometimes $p=1$ or 2, or a value between 1 and 2 may be used to represent scattering from vegetation. The model simulation results were fit to this simple model to estimate σ° and p for both Lhh and Lhv polarizations.

4.3. Biomass estimation

Table 1 lists the biomass data for forest stands used in this study. Several stands have exactly the same value of biomass, which occurred because biomass parameters were defined from forest inventory tables. The biomass values are exactly the same for stands with equal age and site index. These tables and methods are in operational use for Russian forest inventory and management.

Positions of the 56 stands were located on the uncorrected and corrected Lhv radar images and the backscattering signatures were extracted. These stands were sorted according to biomass and selected alternately for either model development or testing. Regression relationships were developed between the cube root of total biomass and the averaged radar signature similarly to the method described by Ranson and Sun (1997a). The biomass levels of these stands were concentrated in low and high ends of the range, which is indicative of the even age of the stands not disturbed by logging or fire. It was assumed the relationships were linear between these levels of biomass and the

Table 2
Parameters used in radar backscatter simulations

Geometry									
	Radius			Length			Probability (%)		
Needle	0.3 mm			2.7 cm			100		
Branch	0.2 cm			15 cm			90		
	0.8 cm			50 cm			8		
	1.6 cm			150 cm			2		
Orientation									
Needle	Vertical preferred ($p(\theta)=4\sin^2\theta/\pi$, $\theta\in(0^\circ, 90^\circ)$ is the zenith angle of the long axis)								
Branch zenith angle (°)	10	20	30	40	50	60	70	80	90
Probability (%)	1.5	2	1.5	3	14	25	22	14	17
Density									
Needle: 23000/m^3					Branch: 120/m^3				
Dielectric constants (real, imaginary)									
Needle	(18.03, 6.10)								
Branch	(15.38, 5.29)								
Trunk	(6.68, 2.07)								
Soil surface	(10.0, 2.0) Roughness: standard deviation of surface height $\sigma=2.5$ cm, surface correlation length $l=18$ cm								

derived equations were used to convert the Lhv images to biomass maps.

5. Results

5.1. Terrain correction with a DEM

In this study, we first corrected the dependence of illuminated pixel area within the SIR-C image on incidence angle using the DEM available from NIMA. We found that the spatial resolution and accuracy of this DEM was not suitable for terrain-effect correction of SIR-C imagery. Fig. 2 is the Lhv image that was corrected using the local incidence angle derived from the DEM. While the correction for large slopes appears to be appropriate, the smaller slopes have not been corrected due to the lower resolution of the DEM data than that of the SIR-C image. Consequently, the method of using backscatter modeling to account for terrain effects on backscatter was used.

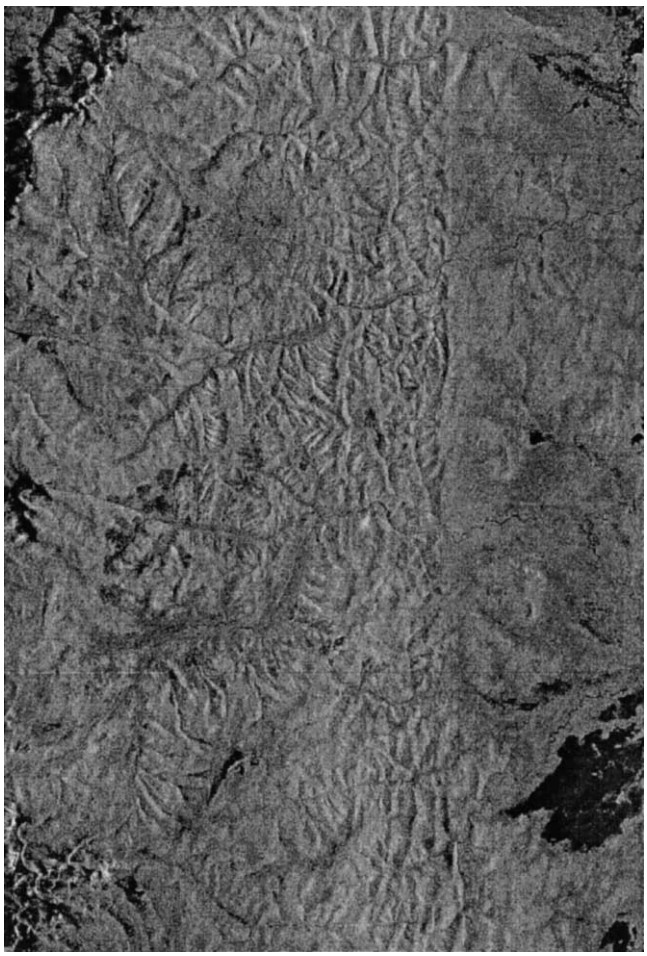

Fig. 2. Terrain-effect-corrected Lhv image using the local radar incidence angle derive from DEM. The large-scale relief was removed from the original Lhv radar image (Fig. 1), but the fine relief remains.

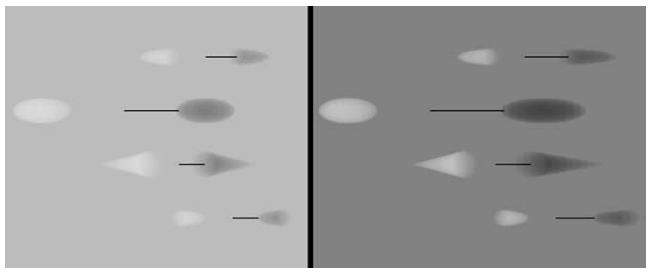

Fig. 3. Simulated radar images (radar looks from the left): left — a horizontal square area with four trees, right — the same area with a 10° slope facing right (away from radar).

5.2. Modeling of the terrain effect

Two simulated Lhh radar images are shown in Fig. 3. The one on the left represents a flat area with four trees of different crown shapes. The radar looks from left to right with an incidence angle of 45°, so the images of the tree crowns (bright), and the crown shadows on the ground (dark) have the same geometry. The other image (on the right) represents the same scene, but the surface has a 10° slope facing to the right and away from radar. Trees are still growing vertical, so the images of the tree crowns did not change, but crowns project longer shadows upon the ground surface. The backscattering from the ground (a rough surface) decreases when the slope faces away from the radar (resulting in a larger local incidence angle effect).

The effect of changing slope on backscatter is demonstrated in Fig. 4. A series of simulated radar images for the stem map discussed above and surface slopes ranging from $-30°$ (30° slope facing radar) to 30° (30° slope facing away from radar) are shown in Fig. 4. The pixel size of the images in Fig. 5 is 0.5×0.5 m in slant range format. The radar incidence angle used was 46.4° (illumination from left), the same as the SIR-C image used for the modeling. The corresponding simulated radar backscattering coefficients for Lhh and Lhv polarizations are shown in Fig. 5. The observed change of

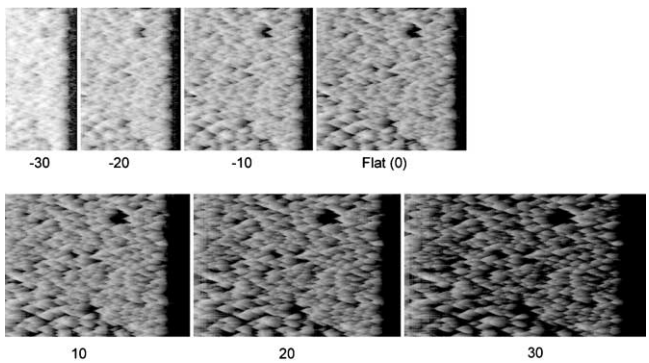

Fig. 4. A series of simulated radar images of a 100×100 m forest stand at various slopes: from left to right, $-30°$, $-20°$, $-10°$, 0° (top row), and 10°, 20°, and 30°. Negative means the slope faces the radar. Radar looks from the left with an incidence angle of 46.4°, relative to a horizontal surface.

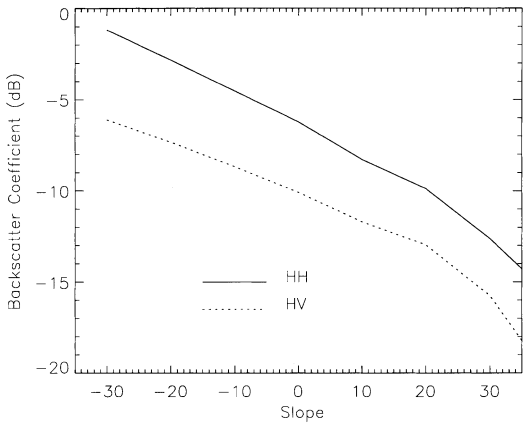

Fig. 5. Backscattering coefficients (Lhh and Lhv) averaged in the 100×100 m stand vs. local incidence angle for the simulated stands shown in Fig. 4.

the backscattering coefficient (the brightness of the images) with changing slope was caused by several factors. The major factors are (1) change of the illuminated area per pixel. This is easily seen in Fig. 5 as the increase in the number of range pixels (resulting in less area illuminated by a pixel) of the scenes between slope angles of $-30°$ and $30°$. (2) Change in tree shadowing. There are more shadows cast by trees visible in the images for slopes facing away from the radar. (3) Change in contribution of surface backscattering because of local incidence angle.

The simulated dependence of radar backscatter on local incidence angle shown in Fig. 5 were used to correct terrain effects. The best fits of the simulated data (Fig. 5) yield the following two equations of the form suggested by Ulaby et al. (1982):

$$\sigma^{\circ}_{\mathrm{hh}}(\theta) = 0.361\cos^{1.78}\theta \qquad r^2 = .93 \tag{3}$$

$$\sigma^{\circ}_{\mathrm{hv}}(\theta) = 0.203\cos^{1.50}\theta \qquad r^2 = .95 \tag{4}$$

In order to check the validity of the simulated curves, a transect (3 pixels wide and 528 pixels long) along the radar range direction for an area with undisturbed forest cover was identified. The Lhh, Lhv backscattering coefficients, and local incidence angle derived from the DEM were extracted from the transect and averaged over the 3 pixels. By examining the SIR-C and the slope images, 29 pixels within

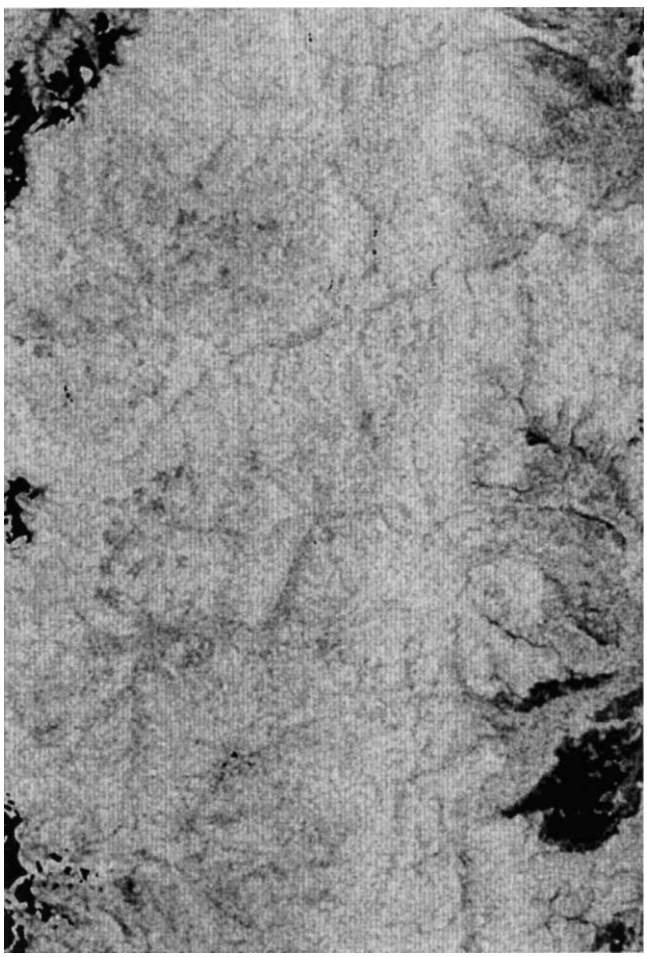

Fig. 6. Terrain-effect-corrected Lhv image using a model-based method described in the Methods section.

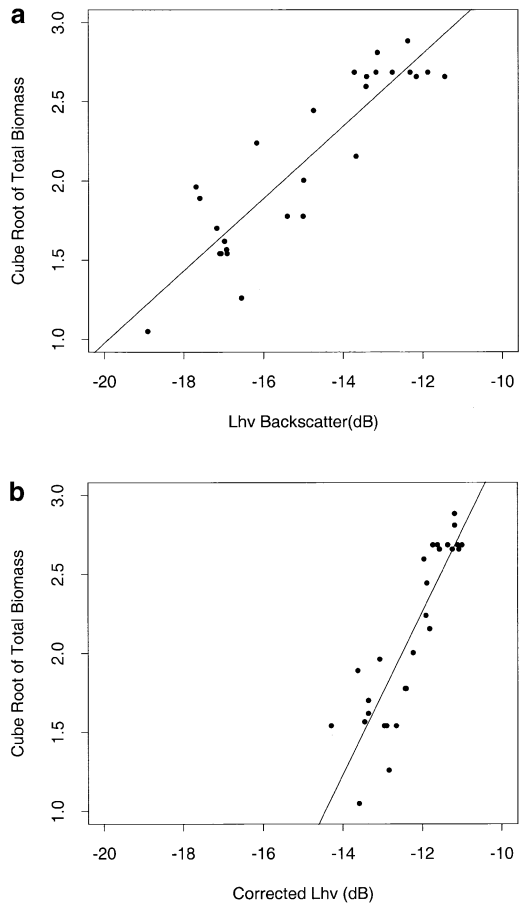

Fig. 7. Regression between biomass and radar backscattering: (a) original Lhv data and (b) terrain-effect-corrected Lhv radar data. See text for these equations.

shadows were deleted from this profile. The same model fits produced the following two equations:

$$\sigma^{\circ}_{hh}(\theta) = 0.285\cos^{1.76}\theta \qquad r^2 = .45 \tag{5}$$

$$\sigma^{\circ}_{hv}(\theta) = 0.073\cos^{1.50}\theta \qquad r^2 = .41 \tag{6}$$

These two equations are very similar to Eqs. (3) and (4), but with poorer fit to the data (i.e., lower r^2). Ideally, equations of this form should be developed for different kinds of land cover type, which will be part of our future modeling efforts. For this study, we used the pair of equations (Eqs. (5) and (6)) to make the terrain correction of the Lhv image. Here, we assume that Eq. (3) is applicable to the SIR-C Lhh image. Eqs. (3) and (5) show that the powers of cosθ, (i.e., p) are very similar (1.78 vs. 1.76), and that the major differences between simulated and actual SAR data may be in σ° (0.361 vs. 0.285). This difference results in only a relative scaling in the corrected Lhv image (see Eqs. (8) and (9)). The modeled σ° for Lhv was not needed for the terrain effect correction (see Eq. (9) below).

5.3. Terrain correction from modeling

For each pixel, Eq. (3) was used to estimate cosθ from the Lhh image data (Eq. (7)):

$$\cos\theta = (\sigma^{\circ}_{hh}(\theta)/0.361)^{1/1.78} \tag{7}$$

If the actual SAR data is different from the simulated data and gives a different value for σ_i° other than the 0.361, the resulting cosθ will be:

$$\cos\theta = (\sigma^{\circ}_{hh}(\theta)/\sigma_i^{\circ})^{1/1.78} = (\sigma^{\circ}_{hh}(\theta)/0.361)^{1/1.78}a \tag{8}$$

where $a=(0.361/\sigma_i^{\circ})^{1/178}$ and accounts for the difference between σ°'s from the simulation (0.361) and radar image (σ_i°).

The purpose of the terrain correction is to bring the Lhv backscattering coefficients at incidence angle θ to a reference incidence angle θ_0. Using Eq. (4) for both θ and θ_0, and taking the ratio of the two results in the following equation:

$$\sigma^{\circ}_{hv}(\theta_0) = \sigma^{\circ}_{hv}(\theta)(\cos\theta_0/\cos\theta)^{1.50}. \tag{9}$$

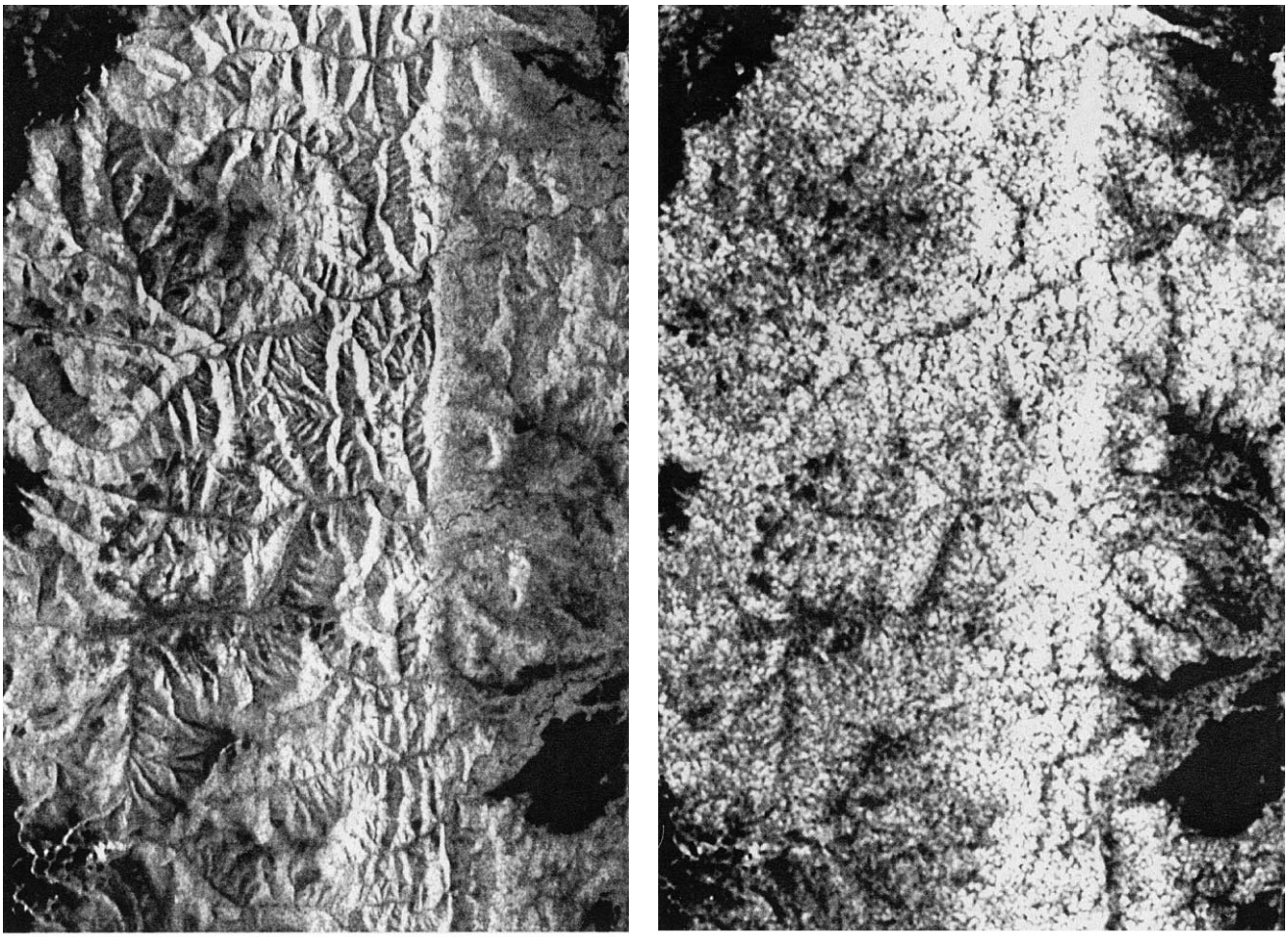

a b

Fig. 8. Biomass maps derived from Lhv vs. biomass relationships for (a) uncorrected and (b) terrain-corrected SIR-C data.

The reference incidence angle θ_0 can be any value, but the natural choice will be the SIR-C radar incidence angle at the image center (46.4°). It can be seen that the uncertainty of $\cos\theta$ caused by the factor a (Eq. (8)) only causes a relative scaling to the corrected Lhv image (Eq. (9)).

The corrected Lhv image using this method (Fig. 6) shows that the terrain pattern was removed (compared with Fig. 1, uncorrected data and Fig. 2 data corrected with the DEM). The low biomass areas, such as clear cuts, top of high mountains, and bare valleys are still identifiable. A threshold limit for Lhv backscattering was set in the correction, so the pixels with Lhv backscattering lower than this limit (shadowing, water surface, or other very low backscattering targets) will not be "corrected." For example, a shadowed area is seen at the upper left of the image in Fig. 1. The dark area at the lower right is known to be a wetland. These areas are the dark features at the upper-left, and lower-right corners of Fig. 6.

5.4. Biomass estimation

Fig. 7a illustrates the relationship of field measured biomass and the uncorrected Lhv backscatter. The relationship developed from corrected Lhv backscatter is shown in Fig. 7b. The equations developed from these data sets are Eqs. (10) and (11):

$$\text{Uncorrected}: B^{1/3} = 5.54 + 0.23\sigma^\circ, \quad r^2 = .81, \quad \mathrm{N} = 28, \tag{10}$$

$$\text{Corrected}: B^{1/3} = 8.45 + 0.67\sigma^\circ, \quad r^2 = .78, \quad \mathrm{N} = 28. \tag{11}$$

Both equations show good linear fit to the data (high r^2). The equation for the corrected data shows greater sensitivity to biomass (larger slope). The lower coefficient of determination (r^2) for corrected data is the result of the reduced range of the backscatter values. After the terrain correction, the backscatter variance within a biomass level was reduced. For example, at biomass 18.8–19.4 kg/m^2 (cube root 2.6–2.7), the range of original Lhv backscatter is about 2.5 dB (Fig. 7a), and that of corrected Lhv is less than 1 dB (Fig. 7b).

The effect of terrain slope on the biomass maps developed from these equations can readily be seen by comparing results using uncorrected (Fig. 8a) and corrected data (Fig. 8b). For the uncorrected data the forward facing slopes yield the highest biomass values, with adjacent, but away-facing slopes showing much lower biomass values. Field observations revealed that these differences were not due to actual biomass, but rather differences in backscatter. In Fig. 8b, the biomass map developed from corrected data shows little effect from the terrain. Biomass differences shown are mostly related to logging, disturbance, or natural vegetation communities, such as wetlands. The two maps are presented with continuous levels of biomass ranging from 0 (black) to ≥ 25 kg/m^2 (white). This upper value range was specified since a small number of points in the image exceeded the maximum biomass levels in the training and testing data.

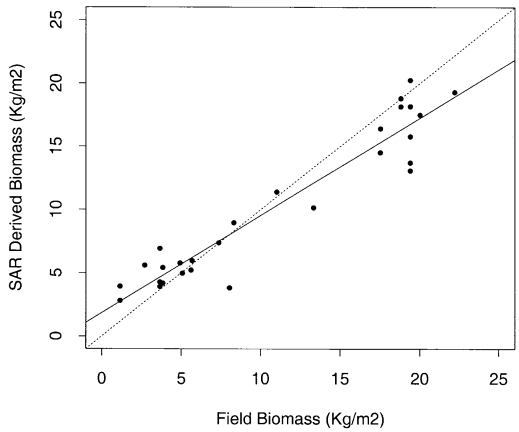

Fig. 9. Comparison between field measurements and SAR predicted biomass for terrain-corrected data. Relationship is SAR Biomass = 1.84 + 0.77 × Field Biomass, r^2=.91, n = 28, RSE = 1.81 kg/m^2.

The comparisons between field biomass test data in Table 1 and predicted biomass developed from applying Eq. (11) to the terrain-corrected data are shown in Fig. 9. The accuracy for the independent set of validation points, given as the root mean square error, was acceptable at 1.81 kg/m^2. The r^2 of .91 was also very good, but the predicted values did not follow a one-to-one relationship with the field measurements. Statistical tests performed on the regression coefficients showed that the slope (0.77) was significantly different from 1.00 and the intercept (1.84) was significantly different from 0.00. Consequently, the predicted biomass estimates are overestimated for low levels and underestimated for higher levels.

6. Conclusions

The effect of terrain on SAR backscatter and subsequent biomass estimation was discussed. We have demonstrated a model-based method for terrain-effect correction of SAR images without using a DEM. However, this method requires multiple polarization SAR data. It seems that if general information on forest structure is available, this method could be used in other areas.

The terrain slope changes the local radar incidence angle, as well as the forest structure perceived by the radar. The dependence of radar backscattering on the slope and aspect (azimuth of the slope) is very complex. Regardless of the methods to be used for terrain effect correction (using DEM or not), certain assumptions have to be made about the nature of the backscatter. The 3-D radar model used in this study provides a tool to simulate the complex structure of the forest stand in mountainous areas. If land cover information is available, this method can be applied to reduce the terrain

effect for different cover type using different equations. If a very good DEM is available, the 3-D model can be used to simulate radar backscattering dependence on terrain, and then used to correct single polarization SAR data.

In this work we based our correction on the model results from a biomass stand of 10 kg/m^2, which resulted in better estimates of midrange biomass values. We will explore how to improve the biomass estimates over the full range by examining low and high biomass cases. In our future studies we will also pursue the combined use of a land cover map, the radar backscatter model, and DEM for terrain effect correction of SAR data for forest parameter retrieval in mountainous areas. Of course full utility of this work awaits the launch of new radars such as the Japanese PALSAR on ALOS or the proposed U.S. multiple channel SAR.

Acknowledgments

The study was supported by NASA Headquarters' Office of Earth Science Terrestrial Ecology Program grant NAG-5-3548 and RTOP 662-92-37. Thanks to Bob Knox of GSFC for the jack pine stem map data from his BOREAS study.

References

Bayer, T., Winter, R., & Schreier, G. (1991). Terrain influences in SAR backscatter and attempts to their correction. *IEEE Transactions on Geoscience and Remote Sensing*, *29* (3), 451–462.

Beaudoin, A., Le Toan, T., Goze, S., Nezry, E., Lopes, A., Mougin, E., Hsu, C. C., Han, H. C., Kong, J. A., & Shin, R. T. (1994). Retrieval of forest biomass from SAR data. *International Journal of Remote Sensing*, *15* (14), 2777–2796.

Bergen, K., Dobson, M. C., Pierce, L. E., & Ulaby, F. T. (1998). Characterizing carbon in a northern forest by using SIR-C/X-SAR imagery. *Remote Sensing of Environment*, *63* (1), 24–39.

Dobson, M. C., Ulaby, F. T., Le Toan, T., Beaudoin, A., Kasischke, E. S., & Christensen, N. (1992). Dependence of radar backscatter on coniferous forest biomass. *IEEE Transactions on Geoscience and Remote Sensing*, *30* (2), 412–415.

Dobson, M. C., Ulaby, F. T., Pierce, L. E., Sharik, T. L., Bergen, K. M., Kellndorfer, J., Kendra, J. R., Li, E., Lin, Y. C., Nashashibi, A., Sarabandi, K., & Siqueira, P. (1995). Estimation of forest biophysical characteristics in northern Michigan with SIR-C/X-SAR. *IEEE Transactions on Geoscience and Remote Sensing*, *33* (4), 877–895.

Fung, A. K. (1994). *Microwave scattering and emission models and their applications*. Norwood, MA: Artech House (573 pp.).

Goering, D. J., Chen, H., Hinzman, L. D., & Kane, D. L. (1995). Removal of terrain effects from SAR satellite imagery of Arctic tundra. *IEEE Transactions on Geoscience and Remote Sensing*, *33* (1), 185–194.

Goyal, S. K., Seyfried, M. S., & O'Neill, P. E. (1998). Effect of digital elevation model resolution on topographic correction of airborne SAR. *International Journal of Remote Sensing*, *19* (16), 3075–3096.

Kellndorfer, J., Pierce, L. E., Dobson, M. C., & Ulaby, F. T. (1998). Toward consistent regional-to-global-scale vegetation characterization using orbital SAR systems. *IEEE Transactions on Geoscience and Remote Sensing*, *36* (5), 1396–1411.

Kurvonen, L., Pulliainen, J., & Hallikainen, M. (1999). Retrieval of biomass in boreal forests from multitemporal ERS-1 and JERS-1 SAR images. *IEEE Transactions on Geoscience and Remote Sensing*, *37* (1), 198–205.

Le Toan, T., Beaudoin, A., Riom, J., & Guyon, D. (1992). Relating forest biomass to SAR data. *IEEE Transactions on Geoscience and Remote Sensing*, *30* (2), 403–411.

Luckman, A. J. (1998). The effects of topography on mechanisms of radar backscatter from coniferous forest and upland pasture. *IEEE Transactions on Geoscience and Remote Sensing*, *36* (5), 1830–1834.

Paloscia, S., Macelloni, G., Pampaloni, P., & Sigismondi, S. (1999). The potential of C- and L-band SAR in estimating vegetation biomass: the ERS-1 and JERS-1 experiments. *IEEE Transactions on Geoscience and Remote Sensing*, *37* (4), 2107–2110.

Ranson, K. J., Saatchi, S., & Sun, G. (1995). Boreal forest ecosystem characterization with SIR-C/X-SAR. *IEEE Transactions on Geoscience and Remote Sensing*, *33* (4), 867–876.

Ranson, K. J., & Sun, G. (1997a). Mapping of boreal forest biomass from spaceborne synthetic aperture radar. *Journal of Geophysical Research*, *102* (D24), 29599–29610.

Ranson, K. J., & Sun, G. (1997b). An evaluation of AIRSAR and SIR-C/X-SAR images for mapping Northern forest attributes in Main, USA. *Remote Sensing of Environment*, *59*, 203–222.

Ranson, K. J., Sun, G., Kharuk, V. I., & Kovacs, K. (2001). Characterization of forests in Western Sayani Mountains, Siberia from SAR data. *Remote Sensing of Environment*, *75*, 188–200.

Rauste, Y. (1990). Incidence-angle dependence in forested and nonforested areas in Seasat SAR data. *International Journal of Remote Sensing*, *11* (7), 1267–1276.

Rignot, E., Way, J. B., Williams, C., & Viereck, L. (1994). Radar estimates of aboveground biomass in boreal forests of interior Alaska. *IEEE Transactions on Geoscience and Remote Sensing*, *32* (5), 1117–1124.

Saatchi, S., & Moghaddam, M. (2000). Estimation of crown and stem water content and biomass of boreal forest using polarimetric SAR imagery. *IEEE Transactions on Geoscience and Remote Sensing*, *38* (2), 697–709.

Saatchi, S., van Zyl, J., & Assar, G. (1995). Estimation of canopy water content in Konza Prairie grasslands using synthetic aperture radar measurements during FIFE. *Journal of Geophysical Research*, *100* (D12), 25481–25496.

Sellers, P. J., Hall, F. G., Kelly, R. D., Black, A., Baldocchi, D., Berry, J., Ryan, M., Ranson, K. J., Crill, P. M., Lettenmaier, D. P., Margolis, H., Cihlar, J., Newcomer, J., Fitzjarrald, D., Jarvis, P. G., Gower, S. T., Halliwell, D., Williams, D., Goodison, B., Wickland, D. E., & Guertin, F. E. (1998). BOREAS in 1997: experiment overview, scientific results, and future directions, BOREAS Special Issue, Journal of Geophysical Research. *Journal of Geophysical Research*, *102* (D24), 28731–28769.

Shi, J. C., & Dozier, J. (1997). Mapping seasonal snow with SIR-C/X-SAR in mountainous areas. *Remote Sensing of Environment*, *59* (2), 294–307.

Stofan, E. R., Evans, D. L., Schmullius, C., Holt, B., Plaut, J. J., van Zyl, J., Wall, S. D., & Way, J. (1995). Overview of results of spaceborne imaging radar-C, X-band synthetic aperture radar (SIR-C/X-SAR). *IEEE Transactions on Geoscience and Remote Sensing*, *33* (4), 817–828.

Sun, G., & Ranson, K. J. (1995). A three-dimensional radar backscatter model of forest canopies. *IEEE Transactions on Geoscience and Remote Sensing*, *33* (2), 372–382.

Ulaby, F. T., Moore, R. K., & Fung, A. K. (1982). *Microwave remote sensing, active and passive*, *vol. III*. Norwood, MA: Artech House (1064 pp.).

Ulander, L. M. H. (1996). Radiometric slope correction of synthetic-aperture radar images. *IEEE Transactions on Geoscience and Remote Sensing*, *34* (5), 1115–1122.

van Zyl, J. J. (1993). The effect of topography on radar scattering from vegetated areas. *IEEE Transactions on Geoscience and Remote Sensing*, *31* (1), 153–160.

Wever, T., & Bodechtel, J. (1998). Different processing levels of SIR-C/X-SAR radar data for the correction of relief induced distortions in mountainous areas. *International Journal of Remote Sensing*, *19* (2), 349–357.